

---

This is an electronic reprint of the original article.  
This reprint may differ from the original in pagination and typographic detail.

Guo , Zhichao; Han, Wenxiang; Zhao, Wenli; Li, Liye; Wang, Baodong; Xiao, Yongfeng;  
Alopaeus, Ville

## The effect of microwave on the crystallization process of magnesium carbonate from aqueous solutions

*Published in:*  
Powder Technology

*DOI:*  
[10.1016/j.powtec.2018.01.038](https://doi.org/10.1016/j.powtec.2018.01.038)

Published: 01/01/2018

*Document Version*  
Peer-reviewed accepted author manuscript, also known as Final accepted manuscript or Post-print

*Published under the following license:*  
CC BY-NC-ND

*Please cite the original version:*  
Guo , Z., Han, W., Zhao, W., Li, L., Wang, B., Xiao, Y., & Alopaeus, V. (2018). The effect of microwave on the crystallization process of magnesium carbonate from aqueous solutions. *Powder Technology*, 328, 358-366. Article 1. <https://doi.org/10.1016/j.powtec.2018.01.038>

---

This material is protected by copyright and other intellectual property rights, and duplication or sale of all or part of any of the repository collections is not permitted, except that material may be duplicated by you for your research use or educational purposes in electronic or print form. You must obtain permission for any other use. Electronic or print copies may not be offered, whether for sale or otherwise to anyone who is not an authorised user.

# The effect of microwave on the crystallization process of magnesium carbonate from aqueous solutions

AUTHOR NAMES: Zhichao Guo<sup>a\*</sup>; Wenxiang Han<sup>a</sup>; Wenli Zhao<sup>a,b</sup>; Liye Li<sup>a</sup>; Baodong Wang<sup>c</sup>; Yongfeng Xiao<sup>c</sup>, Ville Alopaeus<sup>b</sup>

<sup>a</sup>College of Chemical Engineering and Materials Science, Tianjin University of Science & Technology, Tianjin 300475, China.

<sup>b</sup>School of Chemical Technology, Aalto University, Espoo 02150, Finland

<sup>c</sup>National Institute of Clean-and-Low-Carbon Energy, Future Science & Technology City, Changping District, Beijing 102211, China

\*zhichao.guo@tust.edu.cn; phone: +86 22 60602763; fax: +86 22 60600030

**ABSTRACT:**

The effect of microwave on reactive crystallization is investigated with magnesium carbonate as the working substance. In the experiments, magnesium carbonate is precipitated by mixing aqueous magnesium sulfate and sodium carbonate solutions in a MSMR crystallizer located in a microwave reactor. A population balance model along with crystallization kinetics is formulated to assess the influence of microwave energy input on nucleation, growth, agglomeration and breakage during crystallization process. A general high order moment method of classes (HMMC) framework is applied to solve the model numerically. The results show that crystallization kinetics parameters, including the nucleation rate constant ( $k_n$ ), the growth rate constant ( $k_g$ ), the exponent of growth rate ( $g$ ) and the collision efficiency ( $\Psi_{ag}$ ) change significantly due to mass transfer enhancement in microwave field. Meanwhile, the exponent of nucleation ( $n$ ) and the breakage rate constant ( $k_{br}$ ) remain constant or only change slightly. It is further discovered that the crystal suspension attenuates the microwave effect during crystallization process.

**KEYWORDS:** Microwave; Reactive crystallization; Crystallization kinetics; Population balance; Mass transfer

## 1. Introduction

A microwave is a radio wave with a frequency ranging from 300 MHz to 300 GHz.<sup>1</sup> During the last two decades, microwave becomes an efficient and suitable tool in various industrial processes, such as synthesis and processing of chemical materials.<sup>2,3</sup>

Recently, microwave also has attracted considerable attention as a new way to control crystallization process. Asakuma and Miura found growth rate of crystals is improved by microwave field in the anti-solvent crystallization. They claimed that the applied microwave can enhance the diffusion coefficient which governs the liquid to solid mass transfer during crystal growth.<sup>4</sup> Gordon et al. realized that microwave can introduce a fast and uniform nucleation to crystallization system.<sup>5</sup> In addition, the microwave field was also found to change the size and morphology of crystal products.<sup>6,7</sup> In order to achieve a higher yield of crystal products, Rizzuti et al. and Serrano et al. applied the microwave radiation to the crystallization process.<sup>8,9</sup> Wu et al. and Hart et al. found that microwave field can promote the phase transform of crystal.<sup>10,11</sup> Tian et al., Mahmoud et al. and Aquino et al. concluded that microwave can be used to speed up crystal growth during crystallization process.<sup>12,13,14</sup> Asakuma and Miura found that microwave can accelerate the crystal precipitation and control the crystal size.<sup>4</sup> The microwave effect on crystallization has also been reported to change the degree of crystallization.<sup>15,16</sup>

When microwave propagates through a liquid medium, its energy will not only cause temperature increase but also initiate an electromagnetic effect that accelerates the movement and the collision rate of the molecules in the reaction system. As a result, the nucleation and growth of crystals could be improved. Microwave is widely thought to enhance the rate of mass transfer.<sup>4,17,18,19</sup> Meanwhile, Janney et al. and Wilson et al. found that the diffusion coefficients increase in the presence of the microwave electromagnetic effect as well.<sup>20,21</sup> Li et al. found that diffusion acceleration is the main reason for the increase of nucleation rate,<sup>22</sup> and the diffusivity enhancement ( $D_{AB} - D_{AB0}$ ) with energy input ( $E$ ) follows the Arrhenius law.

Despite the fact that microwave has been proven to be an effective method to control crystallization process, to our knowledge, the quantitative study of microwave effect on crystallization kinetics is limited. The aim of this study is to investigate the influence of microwave on the crystallization mechanisms of inorganic salts in a water-based system by analyzing the variation of crystallization kinetic parameters in microwave field.

Magnesium carbonate ( $\text{MgCO}_3$ ) crystals, a typical inorganic salt, were precipitated from the aqueous solution in a laboratory MSMPR crystallizer settled in the cavity of microwave reactor. The experiments were carried out under fixed temperature and various microwave power inputs. A population balance model considering nucleation, growth, agglomeration and breakage was constructed and solved with high order moment method of classes (HMMC).<sup>23,24</sup> The crystallization kinetic parameters, including the nucleation rate constant ( $k_n$ ), the exponent of nucleation ( $n$ ), the growth rate constant ( $k_g$ ), the exponent of growth rate ( $g$ ) and the breakage rate constant ( $k_{br}$ ), were fitted against experimental data. The mechanisms of the microwave effecting on kinetic parameters were discussed as well.

## 2. Theory

Crystallization is a solid–liquid separation technique, in which mass transfer of a solute from the liquid solution to a pure solid crystalline phase occurs. The particle size distribution (PSD) depends on the processes that create new particles ("birth" processes) and destroy existing particles ("death" processes). Birth of new particles can occur due to breakage or splitting, agglomeration and nucleation. Breakage and agglomeration also contribute to death processes.<sup>25</sup> Nucleation, growth and agglomeration are dominated by liquid to solid mass transfer while breakage is mainly affected by turbulent intensity.<sup>26</sup> As previously mentioned, the diffusion coefficient of mass transfer could be significantly influenced by the microwave field. Therefore, The PSD of crystal products may be changed greatly by microwave.

There are three different classes of materials in microwave field: insulators, which are not affected by microwaves, conductors (such as metals) which reflect the energy, but do not heat, and dielectrics (polar molecules, ions) which absorb the energy.<sup>27</sup> With the increase of the weight fraction of inorganic salt, the microwave absorption properties are enhanced, which leads to the enhancement of dielectric and magnetic losses in the solution.<sup>28</sup> In this case, the increase of inorganic salt suspension density may shield the micro-

wave effect on mass transfer during crystallization process. Thus, the influence of microwave energy input on kinetic parameters needs to be analyzed quantitatively to understand the mechanism of crystal formation in microwave field.

In the steady-state crystallization system, the mass balance equation for  $Mg^{2+}$  in the liquid phase can be calculated as follows:

$$Q_{in}c_{in} - R_c V_{disp} - Q_{out}c_{Mg} = 0 \quad (1)$$

where  $c_{in}$  is the concentration of  $Mg^{2+}$  in the inflow;  $c_{Mg}$  is the concentration of  $Mg^{2+}$  in the solution and out-flow;  $Q_{in}$  and  $Q_{out}$  are inflow rate and outflow rate;  $V_{disp}$  is the volume of dispersion. The terms on the left hand side are: 1) liquid feed, 2) crystal mass deposition rate, 3) liquid outlet. The crystal mass deposition rate ( $R_c$ ) can be calculated as follows:<sup>29</sup>

$$R_c = f_v \rho_{MgCO_3} L_0^3 J_N + f_s \rho_{MgCO_3} m_2 G / 2 \quad (2)$$

where  $f_v$  is the volume shape factor and  $f_s$  are the surface shape factor,  $\rho_{MgCO_3}$  is the density of  $MgCO_3$ ,  $L_0$  is primary crystal size and  $m_2$  is 2nd-order moment of size distribution obtained by solving the population balance equation.

Based on the consideration of "birth" and "death" processes, a general form of the population balance equation expressed in particle size as the internal coordinate for an MSMMPR crystallizer in the presence of agglomeration and breakage can be written as:<sup>26</sup>

$$\dot{n}(L)_{in} - \dot{n}(L)_{out} + \frac{\partial}{\partial L} [G(L)n(L)] + J_n = B_{ag}(L) - D_{ag}(L) + B_{br}(L) - D_{br}(L) \quad (3)$$

The terms on the left-hand side are: flow of particles into the control volume, flow of particles out from the control volume, growth along internal coordinate and primary nucleation. The terms on the right-hand side are: birth term by agglomeration, death term by agglomeration, birth term by breakage and death term by breakage. To numerically solve this population balance equation, a general high-order moment method of

classes (HMMC) framework is applied in this paper.<sup>23,24</sup> It is based on conservation of an arbitrary number of moments in the numerical discretization.

After discretizing the internal coordinate space into a finite number of size class ( $NC$ ) and counting the number density of particles ( $Y$ ) belonging to each class, the continuous population balance equation becomes:

<sup>23,24</sup>

$$\frac{1}{V_{disp}} Q_{in} Y_{i,in} - \frac{1}{V_{disp}} Q_{out} Y_{i,out} + \sum_{j=1}^{NC} \xi(L_i, L_j) G(L_j) Y_j + \Omega(L_i) = \sum_{j=1}^{NC} B(L_i, L_j) g(L_j) Y_j + \sum_{j=1}^{NC} \sum_{k=1}^{NC} \chi(L_i, L_j, L_k) F(L_j, L_k) Y_j Y_k - g(L_i) Y_i - Y_i \sum_{j=1}^{NC} F(L_i, L_j) Y_j \quad (4)$$

where  $i, j$  and  $k$  are the indices of particle size class;  $Y_i$  is the particle number density of class  $i$ ;  $g(L, \lambda)$  is the breakage frequency;  $F(L, \lambda)$  is the agglomeration frequency;  $B(L_i, L_j)$  is the breakage table, that determines the contribution of breakage event of particles in  $j$ -th class to particles number in  $i$ -th class;  $\chi(L_i, L_j, L_k)$  is the agglomeration table, that describes the contribution of agglomeration event of particles in  $j$ -th and  $k$ -th class to particles number in  $i$ -th class;  $\xi(L_i, L_j)$  is the growth table, that represents the contribution of growth event of particles in  $j$ -th class to particles number in  $i$ -th class;  $\Omega(L_i)$  is the nucleation table. In this work,  $Y_{i,in}$  is zero since there is no crystals in the inflow. In addition, particle number density in the outflow ( $Y_{i,out}$ ) is equal to the tank averaged particle number density ( $Y_i$ ) due to the typical assumption of well mixing in MSMPR crystallizers.

In stirred tank reactor, the nucleation and growth rates of  $MgCO_3$  can be calculated with power-law functions:<sup>30</sup>

$$J_N = k_n (S)^n \quad (5)$$

$$G = k_g (S)^g \quad (6)$$

where  $J_N$  is the primary nucleation rate;  $k_n$  is the nucleation constant;  $n$  is the exponent of nucleation;  $G$  is the crystal growth rate;  $k_g$  is the growth rate constant;  $g$  is the exponent of growth and  $S$  is the supersatura-

tion.

In the dilute binary solution with charged ions of  $Mg^{2+}$  and  $CO_3^{2-}$ ,  $S$  can be presented as:<sup>31</sup>

$$S = \sqrt{c_{Mg} c_{CO_3}} - \sqrt{K_{sp, MgCO_3}} \quad (7)$$

where  $c$  is the concentration of components in the liquid phase;  $K_{sp}$  is the solubility product of the new formed crystals.<sup>26</sup>

The crystal agglomeration often occurs along with primary nucleation and crystal growth under relatively high supersaturation during reactive crystallization. Besides the properties of surrounding solution, the crystals agglomeration depends on particle-particle and particle-fluid interactions, particle morphology and fluid mixing. Generally, three steps are needed to obtain agglomerates: (a) the collision of two particles, (b) a sufficient time interval during which the two particles stay together with the help of the flow, and (c) the adherence of the two particles caused by supersaturation.<sup>26</sup>

The agglomeration rate,  $F(L_i, L_j)$ , is initially governed by a variety of effect, such as attractive force (Van der Waals theory) and repulsive force (DLVO theory). This balance is significantly influenced by the ionic strength of the solution. Another major effect is due to hydrodynamics or viscous interaction, which tends to hinder the approach of colliding particles. [The agglomeration rate can be expressed as the product of collision frequency function and the collision efficiency:](#)<sup>32,33</sup>

$$F(L_i, L_j) = \left( \frac{2k_B T}{3\mu} \frac{(L_i + L_j)^2}{L_i L_j} + 1.29 \left( \frac{\varepsilon}{\nu} \right)^{1/2} (L_i + L_j)^3 \right) \psi_{ag} \quad (8)$$

where  $k_B$  is Boltzmann constant;  $T$  is temperature;  $\mu$  is dynamics viscosity;  $\varepsilon$  is turbulent energy dissipation;  $\nu$  is kinematic viscosity;  $\psi$  is collision efficiency. [When the crystals are sufficiently small that they neither influence the fluid phase nor are disturbed by fluid shear, the collision frequency can be described by the Brownian kernel.](#)<sup>34</sup> [When particles are sufficiently large compared to shear gradients, collision frequencies are influenced by fluid motion. In the turbulent flow, the collision frequency of the particles can be calcu-](#)

lated by the model proposed by Adachi et al.<sup>35</sup>. In Equation 8, the first term inside the brackets accounts for the Brownian collisions while the second refers to the turbulence-induced collisions.

Hounslow et al. proposed a physically-based semiempirical correlation for collision efficiency during precipitation of inorganic salts in stirred tanks.<sup>36</sup> The collision efficiency  $\psi$  is estimated by:

$$\psi_{ag} = \frac{(\Gamma(\varepsilon)/\Gamma_{50})^\gamma}{1 + (\Gamma(\varepsilon)/\Gamma_{50})^\gamma} \quad (9)$$

$\Gamma_{50}$  and  $\gamma$  are parameters fitted against experimental data.<sup>32</sup> The strength of aggregate,  $\Gamma(\varepsilon)$ , is a function of the energy dissipation, crystal size, apparent yield stress, density of particle, dynamic viscosity of liquid and the growth rate of crystal:

$$\Gamma(\varepsilon) = \frac{\alpha\mu^{1/2}G^2}{\rho_L^{3/2}d_{3,0}^2\varepsilon^{3/2}} \quad (10)$$

where  $\rho_L$  is the density of liquid phase,  $\alpha$  is apparent yield stress,  $\varepsilon$  is turbulent energy dissipation,  $d_{3,0}$  is the volume mean diameter, calculated as the ratio of the 3rd and 0th-order moment.

From Jones, the breakage process is determined by the mechanical strength of crystals and the applied force.<sup>37</sup> According to the study of Marchisio and Fox, the crystal breakage is assumed to be caused by two mechanisms: normal stresses (including crystal-crystal, crystal-impeller, crystal-wall collisions) acting on the surface of the particle and disrupting stresses (including shear stresses, drag stresses and pressure) acting on a crystal agglomerate trapped between two eddies.<sup>38</sup> Particle breakage rate ( $R_{br}$ ) can be factored into two parts. The breakage frequency,  $g(L_i)$ , is the rate function for particle breakage. Daughter size distribution,  $\beta(L_i/L_j)$ , defines the probability that a fragment of size  $L_i$  is formed from the breakage of an  $L_j$ -sized particle. Breakage rate is commonly calculated as a power law function of kinematic viscosity, turbulence dissipation, and agglomerate size.<sup>39,40</sup> By considering dimensional consistency, the breakage law can be reorganized in terms of Kolmogorov length scale ( $\eta$ ) and Kolmogorov time scale ( $\eta_T$ ) as:<sup>33</sup>

$$g(L_i) = k_{br} \left( \frac{L_i}{\eta} \right)^\lambda \eta_T^{-1} \quad (11)$$

where  $k_{br}$  and  $\lambda$  are dimensionless empirical constants. The fragmentation of crystals is assumed as binary breakage. Then the daughter size distribution,  $\beta(L_i/L_j)$ , can be written as:

$$\beta(L_i|L_j) = \frac{180L_i^2}{L_j^3} \left[ \frac{L_i^3}{L_j^3} \left( 1 - \frac{L_i^3}{L_j^3} \right) \right]^2 \quad (12)$$

The parameters used in the simulation are listed in Table 1.

### 3. Experimental

The schematic diagram of experimental apparatus is shown in Figure 1. A laboratory MSMPR crystallizer is applied to investigate the influence of microwave on reactive crystallization. The experiment were carried out in a round-bottom flask with a diameter of 75mm. Magnesium carbonate, precipitated by mixing aqueous solutions of magnesium sulfate and sodium carbonate, was used as the working substance.

The microwave is emitted from a 2450MHz microwave reactor (CEM-Discover), which produces a highly defined and homogeneous microwave field by its circular design of the waveguide to focus the microwave energy towards the reaction vessel. The cooling system and the infrared temperature sensor on the microwave reactor keep temperature of the crystallizer constant. Cooling air is pumped into the system by an air compressor during the crystallization process. By the adjustment of airflow rate, the heat produced by energy input can be eliminated quickly. The temperature of the system is accurate to  $\pm 0.1^\circ\text{C}$ . Thus, the crystallization processes run under consistent microwave power and fixed temperature.

To test the change and the deviation of temperature inside the reactor, a kerosene thermometer, which cannot be heated by microwave, is used to measure the temperatures at different points inside the reactor. It is found that the temperature keeps at  $25.0^\circ\text{C}$  during the experimental process. This means that the heat generated by microwave is removed instantly and the temperature is uniform inside the reactor.

Five levels of displayed power values (0W, 2W, 4W, 6W, 8W) were selected to investigate the influence of microwave on the crystallization kinetics. Since microwave radiation has dielectric loss in the system, the energy obtained by the liquid medium is actually smaller than the displayed value of power input. The correlation between displayed power value and the real energy input obtained by crystallization system is established by measuring the rate of temperature increase inside an isolated vessel. When the change of temperature on heat capacity is ignored, the energy input can be calculated from the arithmetic product of the temperature increase rate, the heat capacity and the solution weight in the isolated vessel. The heat capacity of MgCO<sub>3</sub>-NaSO<sub>4</sub> aqueous solution with different concentrations varies from 2.68 to 2.79 J·g<sup>-1</sup>·K<sup>-1</sup> at 25.0°C, which can be measured and calculated from the mixture of NaCO<sub>3</sub> and MgSO<sub>4</sub> solutions with the concentrations of 0.1mol/L, 0.125mol/L, 0.15mol/L, 0.175mol/L, 0.2mol/L and 0.225 mol/L respectively. The relationship between displayed power values of microwave reactor and energy inputs to different MgCO<sub>3</sub>-NaSO<sub>4</sub> aqueous solutions is shown in Figure 2. It is found that change of salt concentrations in the solution causes the highest calculated difference of real energy input (*E*) when the displayed power values of microwave reactor is 8W . The value of this difference is 0.33W, which is smaller than 5% of real energy input. Thus, an average value of heat capacity, which is 2.74 J·g<sup>-1</sup>·K<sup>-1</sup>, is adopted in this experiment to calculate the real energy input (*E*), in order to decrease the calculated value deviation caused by the change of heat capacity to less than 3%. The corresponding real energy input value at a [given](#) power value [displayed on the microwave emitter](#) can be obtained. When displayed power value of microwave reactor is 2W, the real energy input value is 1.95W, 4W: 3.88W; 6W:5.83W; 8W:7.78W.

To study the crystallization kinetics, magnesium sulfate solution and sodium carbonate solution with the same molar concentration were added into MSMMPR crystallizer at equal flow rates of 3.25 mL/min by two peristaltic pumps. The product flow containing magnesium carbonate crystals, sodium sulfate and water, was pumped out by another peristaltic pump with a flow rate of 6.5 mL/min. The online high-speed camera

was used to monitor the system to obtain a constant liquid level. Six feed concentrations (0.1mol/L, 0.125mol/L, 0.15mol/L, 0.175mol/L, 0.2mol/L and 0.225 mol/L) of magnesium sulfate and sodium carbonate solutions were used in each energy input level to study the influence of microwave on crystallization kinetics. The residence time is defined as the ratio between reactor volume and input flow rate. During the process, the temperature was kept at 25°C and the agitation rate was maintained at 300 rpm. The system was operated for ten residence times to achieve the steady-state condition.

The sample of MgCO<sub>3</sub> crystals was analyzed by a BECKMAN COULTER™ particle size analyzer. In order to ensure the repeatability of measurement, PSD of three parallel samples from experiments under identical operating conditions were taken and tested. The Sauter Mean Diameter of crystals ( $d_{32}$ ), defined as the ratio between third and second-order of moments, is used as the indicator for repeatability test. It is found that the highest difference of  $d_{32}$  value between different measurements is less than 5%. Thus, the measurement results has high consistency. Meanwhile, the concentration of Mg<sup>2+</sup> in steady-state solution was obtained by titration with EDTA. The intermediate value of  $d_{32}$  in three measurements together with concentration of Mg<sup>2+</sup> were selected as experimental data for validation of the modeling results.

#### 4. Results and discussion

From the presented model of reactive crystallization, Mg<sup>2+</sup> concentration in the liquid phase and  $d_{32}$  of crystal product were predicted at different feeding concentrations and microwave energy inputs. The unknown parameters for crystallization ( $k_n$ ,  $n$ ,  $k_g$ ,  $g$  and  $k_{br}$ ) were fitted against the experimental data with least squares method (lsqnonlin function) in Matlab R2017a. The objective function of the fitting algorithm is defined as:

$$F = w_1 \frac{d_{32,mod} - d_{32,exp}}{d_{32,exp}} + w_2 \frac{C_{Mg,mod} - C_{Mg,exp}}{C_{mg,exp}} \quad (13)$$

where subscripts *mod* and *exp* represent the modelling and experimental results respectively;  $w_1$  and  $w_2$  are weighting factors for  $d_{32}$  and  $c_{Mg}$ . In addition, the parameter fitting results could be very sensitive if there was a significant magnitude difference between variables. Therefore, nondimensionalization is performed by introducing average experimental values in Eq.(13). The nonlinear least squares fitting procedure can be carried out as:

$$\min_{\mathbf{x}} \|F(\mathbf{x})\|_2^2 = \min_{\mathbf{x}} (F_1(\mathbf{x})^2 + F_2(\mathbf{x})^2 + \dots + F_n(\mathbf{x})^2) \quad (14)$$

where  $\mathbf{x}$  is the vector of unknown parameters;  $n$  is the total number of experiments used for parameter fitting. After giving initial values, the final parameters with 95% confidence intervals were obtained and presented in Table 2.

The experimental results and the prediction of  $Mg^{2+}$  concentration in steady-state solution as a function of the inflow concentration are shown in Figure 3. As regards the feeding concentration, it is observed that feed solution with higher concentration pumped into the reactor during a given time interval leads to a raise of  $Mg^{2+}$  concentration, which determines the supersaturation of crystallization. According to the mass balance of components, the feeding contributes to the accumulation of the amount of  $Mg^{2+}$  while discharging and crystal mass deposition during crystallization cause the decrease of  $Mg^{2+}$ . It can be deduced that the effect of feeding procedure on the steady state concentration of  $Mg^{2+}$  prevails over the influence of discharging and crystallization under the investigated operating conditions. In respect of microwave, the concentration of  $Mg^{2+}$  in steady-state solution decreases with an increasing microwave energy input at a given inflow concentration. According to previous studies,<sup>20,21,22</sup> the diffusion coefficient of system is enhanced significantly by the microwave electromagnetic effect. Thus, the mass transfer rate of  $MgCO_3$  units from solution to crystal surface should be increased accordingly. Meanwhile, the rate of solid deposition, namely surface integration, governed by the diffusion and collision process of  $Mg^{2+}$  and  $CO_3^{2-}$  should be enhanced as well. Therefore, the higher microwave power input causes the decrease of concentration in steady-state solution.

The above phenomenon is similar to the observation in Ji et al. s' works.<sup>18,19</sup>

The experimental results and the prediction of  $d_{32}$  under various inflow concentrations and energy inputs are shown in Figure 4. The results show that inflow with higher concentration produces crystals with larger size. The reason of this phenomenon is the increase of supersaturation, which improves both the crystal growth rate and the agglomeration rate between crystals in the system. In addition,  $d_{32}$  of  $\text{MgCO}_3$  crystals is also affected by microwave. With the increase of microwave energy input,  $d_{32}$  is increased significantly at a given inflow concentration. Since the diffusion coefficient is increased significantly, both the collision rate between  $\text{Mg}^{2+}$  and  $\text{CO}_3^{2-}$  to form  $\text{MgCO}_3$  crystal units and the diffusion process of  $\text{MgCO}_3$  units to crystal surface, namely crystal growth, can be accelerated simultaneously in microwave field. According to Equation 9 and Equation 10, the collision efficiency, dominating the agglomeration rate, is proportional to crystal growth rate. Similar result can be found in the study of Mersmann that the agglomeration rate is directly proportional to the diffusivity of units.<sup>26</sup> The increase of agglomeration rate leads to larger crystals. Therefore,  $d_{32}$  grows with the increase of microwave energy input.

From Figure 3 and 4, it can be concluded that both of the microwave and feeding concentration have a strong influence on the steady state concentration of  $\text{Mg}^{2+}$  and the size of final crystal products. Moreover, the presented model is capable of predicting the experimental results of reactive crystallization under microwave field. The parameters obtained from this model, including the nucleation rate constant ( $k_n$ ), the exponent of nucleation ( $n$ ), the growth rate constant ( $k_g$ ), the exponent of growth ( $g$ ), and the breakage rate constant ( $k_{br}$ ), are reliable.

The concentrations of  $\text{Mg}^{2+}$  in steady-state solution and Sauter Mean Diameters ( $d_{32}$ ) with the inflow concentrations of 0.1mol/L, 0.125mol/L, 0.15mol/L, 0.175mol/L, 0.2mol/L and 0.225 mol/L are used to fit the crystallization kinetic parameters at each microwave energy input level. The crystallization kinetic parameters (with 95% confidence intervals) obtained from the simulation are listed in Table 2. From Table 2, it is

observed that the ranges of 95% confidence intervals are distributed on the second or the third digit position of the kinetic parameters. This proves that the simulation results and experimental data have high consistency.

As it is shown in Table 2 and Figure 5, the nucleation rate constant ( $k_n$ ) increases quickly with the increase of energy input from 0W to 7.78W. This is to be expected as the diffusion coefficient ( $D_{AB}$ ) rises with the energy input in line with an Arrhenius term.<sup>22</sup> However, the trend line of the nucleation rate constant ( $k_n$ ) plotted against microwave energy inputs ( $E$ ) partially deviates from Arrhenius form, which means the microwave effect on  $k_n$  is interfered in crystallization system. According to the study of Zou et al.,<sup>28</sup> the existence of inorganic salt results in the enhancement of dielectric and magnetic losses in the solution. From the observation of Figure 3, the concentration of  $Mg^{2+}$  decreases quickly with the increase of microwave energy input. Thus, the suspension density of  $MgCO_3$  increases synchronously. The solution with higher solid suspension density could absorb more energy from microwave input. After first nucleation stage, this phenomenon shields the effect of microwave on nucleation rate at high energy input levels.

From Table 2, it is observed that the exponent of nucleation ( $n$ ) remains constant or changes only slightly. This result is consistent with the former study,<sup>41</sup> claiming that microwave does not increase the exponent of nucleation significantly during neither homogeneous nucleation nor heterogeneous nucleation.

The growth rate constant ( $k_g$ ) as a function of microwave energy inputs ( $E$ ) is shown in Figure 6. It can be observed that the growth rate constant ( $k_g$ ) rises with the increasing microwave energy input. The above phenomenon is also caused by diffusion process acceleration, which leads to the increase of the collision rate between  $Mg^{2+}$  and  $CO_3^{2-}$ . Meanwhile, the diffusion process of units transporting from the bulk of the fluid phase through a stagnant film to the solid surface is increased either. With the compound action of the electromagnetic shielding effect caused by  $MgCO_3$  crystals and diffusion acceleration caused by microwave, the trend line of  $k_g$  plotted against microwave energy inputs ( $E$ ) forms a concave curve.

The plots of the exponent of growth ( $g$ ) vs microwave energy input ( $E$ ) are shown in Figure 7. The exponent of growth ( $g$ ) decreases from 1.52 to 1.09 quickly with the increase of energy input ( $E$ ) from 0W to 7.78W. Mullin and Mersmann reported that the inorganic salts crystallization from aqueous solution gives an overall exponent of growth, in the range of 1 to 2.<sup>26, 42</sup> When  $g$  approaches 1, the crystallization process is controlled by the diffusional operation, and when  $g$  approaches 2, the crystallization process is controlled by the surface integration. With the increase of microwave energy input from 0W to 7.78W, the exponent of growth ( $g$ ) decreases from 1.52 to 1.09. This means that with the energy input increase, the crystal growth is increasingly limited by diffusion process. Two reasons may cause above phenomenon. Firstly, according to Mullin and Mersmann,<sup>26, 42</sup> the process of unit integration into the lattice can be considered as a surface reaction process. Since microwave increases both the reaction rate and mass transfer, from the change of the exponent of growth ( $g$ ) with microwave energy input, it can be conclude that the reaction rate increases more quickly with energy input than the mass transfer in microwave field. Secondly, the  $Mg^{2+}$  concentration decreases with the increase of microwave energy input. This means the concentration of  $MgCO_3$  units in the bulk solution falls. The  $MgCO_3$  units must firstly be transported by diffusion from the bulk of the solution to the immediate vicinity of the crystal surface, and then, integrate to the kink on the crystal surface. Because the units transported to the immediate crystal surface are not sufficient, the kink density becomes relatively high. Therefore, crystal growth is controlled by diffusion process.

The influence of energy input on  $Mg^{2+}$  concentration and  $d_{32}$  shows that the crystal growth rate increase with rising microwave energy input. This is to be expected on account of the mass transfer increase. Despite the decrease of the exponent growth ( $g$ ), the increase of the growth rate constant ( $k_g$ ) still speeds up the crystal growth in microwave field.

From Table 2, it can be observed that the breakage rate constant ( $k_{br}$ ) remains constant or only changes slightly. This means that microwave does not influence the breakage process during the crystallization pro-

cess. Since microwave is a kind of electromagnetic wave, which cannot enhance the turbulent intensity in crystallization system, the impact-induced stresses and fluid-induced stresses remain unchanged after microwave is applied to crystallization system. Consequently, compared to agitation, microwave provides a proper solution to increase the diffusion process while avoiding breakage of crystal agglomerates during the reactive crystallization.

The change of collision efficiency ( $\psi_{ag}$ ) at various energy inputs during crystallization process is shown in Figure 8. From this figure, it is observed that  $\psi_{ag}$  is enhanced significantly by the increasing energy input. Thus, the agglomeration between crystals is enhanced after microwave is applied to the system. The agglomeration rate constant can be calculated as the product of collision efficiency and collision rate constant. Collision efficiency depends on the ability of two newly collided particles to cement themselves together.<sup>36</sup> Thus, both the growth rate of crystals and the mass diffusion process may influence the collision efficiency. From Mersmann,<sup>26</sup> the agglomeration depends on kinetic processes, mainly crystal growth, in supersaturated solutions. This conclusion concurs with Equation 9 and 10. From Equation 10, the crystal growth rate ( $G$ ) determines the strength of aggregate ( $I$ ). During initial stage of reactive crystallization, a significant increase of the strength of aggregate ( $I$ ) caused by faster crystal growth in presence of microwave may enhance the collision efficiency towards 1. This means two newly collided particles have more chance to cement themselves together. Thus, the increased microwave energy input leads to a higher collision efficiency.

To verify the above analysis of microwave effects on nucleation, crystal growth, breakage and agglomeration during crystallization process, three crystal SEM images with similar magnitude of enlargement are compared in Figure 9. In this figure, Image A and B include crystals with the inflow concentration of 0.1 mol/L, but the energy input of 0W and 7.78W respectively. Image C includes the crystals from experiments with the inflow concentration of 0.225 mol/L and the energy input of 7.78W.

It is observed from this figure that majority of monocrystals in Image A are smaller than monocrystals in

Image B. This indicates that the sizes of monocrystals increase with energy input. Meanwhile, the size of monocrystals in Image C rise with the enhancement of both supersaturation and microwave energy input.

When the inflow concentration is 0.1 mol/L, with the enhancement of microwave energy input from 0W to 7.78W, the value of collision efficiency is increased from 0.65 to 0.77. With the increase of collision efficiency, the monocrystals have more tendency to agglomerate. Based on the visual classification method developed by Faria et al<sup>43</sup>, it is observed that majority of crystals in Image A can be defined as small agglomerates and medium agglomerates. However, in Image B, the complexity of agglomerates crystals increases from small and medium to large. Since the agglomeration degree increases with the increase of the complexity of the crystal<sup>44</sup>, it can be concluded that the monocrystals tend to agglomerate after microwave is introduced to the system. From the comparison between Image C and A, it is found that with the increase of supersaturation, the complexity of agglomerated crystals increases from small and medium to large as well. The crystals also have a strong tendency to agglomerate in high supersaturated solutions

In general, the SEM observations in Figure 9 concur with the experimental and simulation results of crystal size in Figure 4. Thus, the effect of microwave field on the reactive crystallization are verified. In addition, the mathematical model proposed for reactive crystallization as well as the kinetics parameters fitted against experimental data are reliable.

## 5. Conclusion

This paper shows a quantitative study of microwave field on reactive crystallization at fixed temperature. A population balance model coupled with corresponding experimental validations are used to investigate the influence of microwave on nucleation, growth, agglomeration and breakage during crystallization processes. A general high-order moment conserving method of classes (HMMC) is adopted to solve the model numerically. The parameters for MgCO<sub>3</sub> crystallization ( $k_n$ ,  $n$ ,  $k_g$ ,  $g$  and  $k_{br}$ ) were fitted against the experimental data by the least square method with 95% confidence intervals.

It is found that the exponent of nucleation ( $n$ ) and the breakage rate constant ( $k_{br}$ ) remain constant or change only slightly **under microwave of various intensities**. However, the nucleation rate constant ( $k_n$ ), the growth rate constant ( $k_g$ ) and the collision efficiency ( $\Psi_{ag}$ ) **increase** significantly with **higher** microwave energy input. Furthermore, the growth rate exponent ( $g$ ) **decreases**. The reason for above **phenomena** is the increase of mass transfer rate in microwave field. Therefore, compared to agitation, microwave provide a proper **method** to **improve the crystal growth while** avoiding **particle breakage** in crystallization system. **Compared with cleared solution**, a higher microwave energy input is required to achieve the same enhancement of crystal **growth due to** the electromagnetic shielding effect caused by **the increasing** suspension density of  $MgCO_3$  crystals **during crystallization**. The above conclusions are further proved by the comparison of SEM images of crystals **formed under** different **microwave** energy inputs and the inflow concentrations.

## Notation

$\alpha$	=	apparent yield stress
$\varepsilon$	=	turbulent energy dissipation
$\rho$	=	density
$\mu$	=	dynamics viscosity
$\nu$	=	kinematic viscosity
$\psi$	=	collision efficiency
$\eta$	=	Kolmogorov length scale
$\eta_T$	=	Kolmogorov time scale
$\Gamma$	=	strength of aggregate
$\tau$	=	residence time

$\beta(L_i/L_j)$	=	the daughter size distribution
$\chi(L_i, L_j, L_k)$	=	agglomeration table
$\zeta(L_i, L_j)$	=	growth table
$\Omega(L_i)$	=	nucleation table
$B(L_i, L_j)$	=	breakage table
$c$	=	concentration
$F(L_i, L_j)$	=	agglomeration rate
$f_v$	=	volume shape factor
$f_s$	=	surface shape factor
$g$	=	the exponent of growth
$G$	=	crystal growth rate
$g(L_i)$	=	breakage frequency
$J_N$	=	nucleation rate
$K_{sp}$	=	solubility product
$k_B$	=	Boltzmann constant
$k_n$	=	nucleation rate constant
$k_g$	=	growth rate constant
$L_0$	=	particle size distribution
$L$	=	particle size
$m_2$	=	2nd-order moments of size distribution
$n$	=	the exponent of nucleation
$Q$	=	flow rate
$R_c$	=	crystal mass deposition rate

$S$  = supersaturation  
 $T$  = temperature  
 $V$  = volume  
 $w_1$  = weighting factors for  $d_{32}$   
 $w_2$  = weighting factors for  $c_{Mg}$   
 $\mathbf{x}$  = the vector of unknown parameters  
 $Y$  = particle number density

### subscripts

$ag$  = agglomeration  
 $br$  = breakage  
 $disp$  = dispersion  
 $exp$  = experimental results  
 $i, j, k$  = index of particle size class  
 $in$  = inflow rate  
 $L$  = liquid phase  
 $mod$  = modelling results  
 $out$  = outflow rate

### Reference:

- (1) Gabrielli, C.; Maurin, G.; Poindessous, G.; Rosset, R. Nucleation and growth of calcium carbonate by an electrochemical scaling process. *J. Cryst. Growth.* **1999**, 200, 236-250.
- (2) Leonelli, C.; Mason, T.J. Microwave and ultrasonic processing: Now a realistic option for industry.

Chem. Eng. Process. **2010**, 49, 885-900.

(3) Estel, L.; Poux, M.; Benamara, N.; Polaert, I. Continuous flow-microwave reactor: Where are we?.

Chem. Eng. Process. **2017**, 113, 56-64.

(4) Asakuma, Y.; Miura, M. Effect of microwave radiation on diffusion behavior of anti-solvent during crystallization. J. Cryst. Growth. **2014**, 402, 32-36.

(5) Gordon, J.; Kazemian, H.; Rohani, S. Rapid and efficient crystallization of MIL-53(Fe) by ultrasound and microwave irradiation, Micropor Mesopor Mat. **2012**, 162, 36-43.

(6) Liu, H.; Xiang, K.; Yang, B.; Yang, S.; Li, Q.Z. Microwave intensified synthesis of regular shaped sodium bisulfate crystal, Chem. Eng. Process. **2015**, 95, 208-213.

(7) Rodríguez-Clemente, R.; Gómez-Morales, J. Microwave precipitation of CaCO<sub>3</sub> from homogeneous solutions. J. Cryst. Growth. **1996**, 169, 339-346.

(8) Rizzuti, A.; Leonelli, C. Crystallization of aragonite particles from solution under microwave irradiation. Powder Technol. **2008**, 186, 255-262.

(9) Serrano, D.P.; Uguina, M.A.; Sanz, R.; Castillo, E.; Rodríguez, A.; Sánchez, P. Synthesis and crystallization mechanism of zeolite TS-2 by microwave and conventional heating. Micropor Mesopor Mat. **2004**, 69, 197-208.

(10) Wu, W.W.; Cai, J.C.; Wu, X.H.; Liao, S.; Wang, K.T.; Tao, L. Nanocrystalline LaMnO<sub>3</sub> preparation and kinetics of crystallization process. Adv. Powder Technol. **2013**, 24, 154-159.

(11) Hart, J.N.; Menzies, D.; Cheng, Y.B.; Simon, G.P.; Spiccia, L. A comparison of microwave and conventional heat treatments of nanocrystalline TiO<sub>2</sub>. Sol. Energy Mater. Sol. Cells. **2007**, 91, 6-16.

(12) Tian, F.; Wu, Z.S.; Chen, Q. Y.; Yan, Y.J.; Cravotto, G.; Wu, Z. L. Microwave –induced crystallization of AC/TiO<sub>2</sub> for improving the performance of rhodamine B dye degradation. Appl. Surf. Sci. **2015**, 351, 104-112 .

- (13) Mahmoud, M.M.; Thumm, M. Crystallization of lithium disilicate glass using high frequency microwave processing. *J. Eur. Ceram. Soc.* **2015**, *35*, 2915-2922.
- (14) Aquino, J.M.; Rocha-Filho, R.C. Microwave-assisted crystallization into anatase of amorphous TiO<sub>2</sub> nanotubes electrochemically grown on a Ti substrate. *Mater. Lett.* **2014**, *126*, 52-54.
- (15) Choi, B.K.; Jang, S.W.; Kim, E.S. Dependence of microwave dielectric properties on crystallization behaviour of CaMgSi<sub>2</sub>O<sub>6</sub> glass-ceramics. *Mater. Res. Bull.* **2015**, *67*, 234–238.
- (16) Kiani, M.; Ebadzadeh, T. Effect of mechanical activation and microwave sintering on crystallization and mechanical strength of cordierite nanograins. *Ceram. Int.* **2015**, *41*, 2342–2347.
- (17) Ogunniran, O.; Binner, E.R.; Sklavounos, A.H.; Robinson, J.P. Enhancing evaporative mass transfer and steam stripping using microwave heating. *Chem. Eng. Sci.* **2017**, *165*, 147-153.
- (18) Ji, Z.G.; Wang, J.; Hou, D.Y.; Yin, Z.F.; Luan, Z.K. Effect of microwave irradiation on vacuum membrane distillation, *J. Membrane Sci.* **2013**, *429*, 473-479.
- (19) Ji, Z.G.; Wang, J. Effect of microwave irradiation on typical inorganic salts crystallization in membrane distillation process, *J. Membrane Sci.* **2014**, *455*, 24-30.
- (20) Janney, M.A.; Kimrey, H.D.; Schmidt, M.A.; Kiggans, J.O. Grain growth in microwave- Annealed Alumina, *J. Am. Ceram. Soc.* **1991**, *74* , 1675–1681.
- (21) Wilson, B.A.; Lee, K.Y.; Case, E.D. Diffusive crack-healing behavior in polycrystalline alumina: a comparison between microwave annealing and conventional annealing. *Mater. Res. Bull.* **1997**, *32* , 1607–1616.
- (22) Li, L.; Guo, Z.; Han, W.; Wang, Q. The effect of microwave on the primary nucleation of CaSO<sub>4</sub> from aqueous solutions, *Powder Technol.* **2017**, *317*, 189-196.
- (23) Alopaeus, V.; Laakkonen, M.; Aittamaa, J. Solution of population balances with growth and nucleation by high order moment-conserving method of classes. *Chem. Eng. Sci.* **2007**, *62*, 2277-2289.

- (24) Alopaesus, V.; Laakkonen, M.; Aittamaa, J. Solution of population balances with breakage and agglomeration by high-order moment-conserving method of classes. *Chem. Eng. Sci.* **2006**, 61, 6732-6752.
- (25) Ramkrishna, D. *Population Balances: Theory and Applications to Particulate Systems in Engineering*. Academic Press, San Diego. 2000.
- (26) Mersmann, A. *Crystallization Technology Handbook*. Second Edition. Marcel Dekker, New York. 2001.
- (27) Basak, T.; Priya, A.S. Role of metallic and ceramic supports on enhanced microwave heating processes. *Chem. Eng. Sci.* **2005**, 60, 2661-2677.
- (28) Zou, Z.; Xuan, A.G.; Yan, Z.G.; Wu, Y.X.; Li, N. Preparation of Fe<sub>3</sub>O<sub>4</sub> particles from copper/iron ore cinder and their microwave absorption properties. *Chem. Eng. Sci.* **2010**, 65, 160-164.
- (29) Jones, A.G.; Hostomsky, J.; Zhou, L. On the effect of liquid mixing rate on primary crystal size during the gas-liquid precipitation of calcium carbonate. *Chem. Eng. Sci.* **1992**, 47, 3817–3824.
- (30) Zhao, W.; Han, B.; Jakobsson, K.; Louhi-Kultanen, M.; Alopaesus, V. Mathematical model of precipitation of magnesium carbonate with carbon dioxide from the magnesium hydroxide slurry. *Comput. Chem. Eng.* **2016**, 87, 180-189.
- (31) Dirksen, J.A.; Ring, T.A. Fundamentals of crystallization: Kinetic effects on particle size distributions and morphology. *Chem. Eng. Sci.* **1991**, 46, 2389-2427.
- (32) Marchisio DL; Vigil R D; Fox RO. Implementation of the quadrature method of moments in CFD codes for aggregation-breakage problems. *Chem Eng Sci.* **2003**, 58, 3337-3351.
- (33) Zhao, W.; Buffo, A.; Alopaesus; V.; Han, B.; Louhi-Kultanen, M. Application of the Compartmental Model to the Gas - Liquid Precipitation of CO<sub>2</sub>-Ca(OH)<sub>2</sub> Aqueous System in a Stirred Tank. *AIChE J.* **2017**, 63, 378-386.
- (34) Von Smoluchowski, M. (1917). *Versuch einer mathematischen Theorie der Koagulationskinetik kolloider Lösungen* (1st ed.). Frankfurt: Geest Portig.

- (35) Adachi, Y., Cohen Stuart, M. A., Fokkink, R. Kinetics of Turbulent Coagulation Studied by Means of End-over-End Rotation. *Journal of Colloid and Interface Science*. **1994**, 165, 310-317.
- (36) Hounslow, M.J.; Mumtaz, H.S.; Collier, A.P.; Barrick, J.P.; Bramley, A.S. A micro-mechanical model for the rate of aggregation during precipitation from solution. *Chem. Eng. Sci.* **2001**, 56, 2543–2552.
- (37) Jones, A.G. *Crystallization Process System*. First Edition. Butterworths-Heinemann, Oxford, 2002.
- (38) Marchisio DL, Fox RO. *Computational Models for Polydisperse Particulate and Multiphase Systems*, 1st Edition. Cambridge University Press, New York. 2013.
- (39) Kramer, T.A.; Clark, M.M. Incorporation of aggregate breakup in the simulation of orthokinetic coagulation, *J. Colloid. Interface Sci.* **1999**, 216, 116–126.
- (40) Wójcik, J.A.; Jones, A.G. Dynamics and stability of continuous MSMPR agglomerative precipitation: Numerical analysis of the dual particle coordinate model. *Comput. Chem. Eng.* **1998**, 22, 535-545.
- (41) Guo, Z.; Li, L.; Han, W.; Li, J.; Wang, B.; Xiao, Y. Interpretation of the microwave effect on induction time during CaSO<sub>4</sub> primary nucleation by a cluster coagulation model. *J. Cryst. Growth*. **2017**, 475, 220-231.
- (42) Mullin, J.W. *Crystallization*. Third Edition. Butterworths-Heinemann, Oxford. 2000.
- (43) Faria, N.; Pons, M.N.; Feyerherm, S.; Rocha, F.A.; Vivier, H. Quantification of the morphology of sucrose crystals by image analysis, *Powder Technology*, **2003**, 133, 54-67.
- (44) Faria, N.; Feyerherm, S.; Rocha, F.A.; Pons, M.N. Modelling agglomeration degree in sucrose crystallization, *Chemical Engineering and Processing: Process Intensification*, **2008**, 47, 1666-1677.

**Figures:**

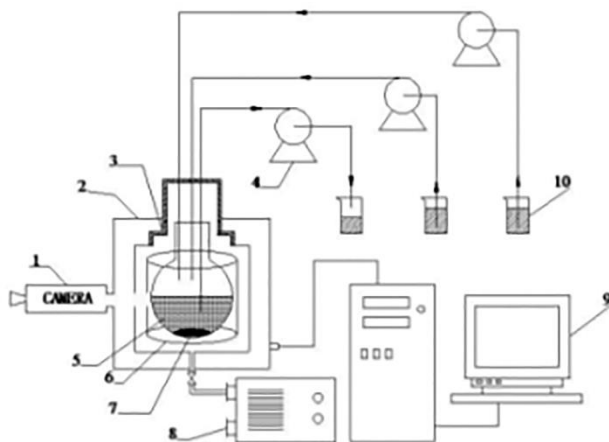


**Fig. 1. The schematic diagram of the experimental set-up.**

- |                             |                      |                     |
|-----------------------------|----------------------|---------------------|
| 1. High speed camera        | 2. Microwave reactor | 3. Top cover        |
| 4. Peristaltic pump         | 5. Crystallizer      | 6. Microwave cavity |
| 7. Magnetic stirrer         | 8. Air compressor    | 9. Computer         |
| 10. Solution storage beaker |                      |                     |

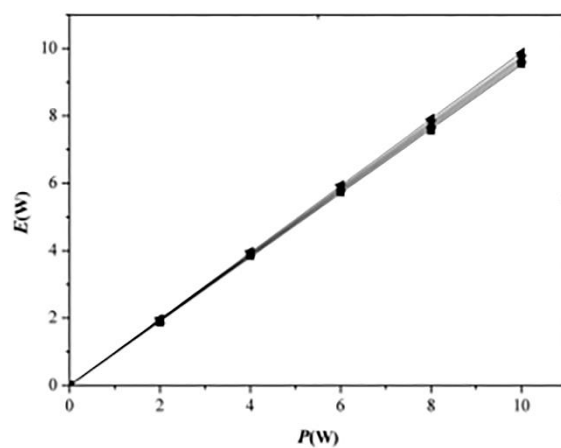


**Fig. 2. Displayed power values of microwave reactor ( $P$ ) vs. energy input ( $E$ ) in solutions with 0.1mol/L, 0.125mol/L, 0.15mol/L, 0.175mol/L, 0.2mol/L, 0.225mol/L input concentrations of  $\text{MgCO}_3$  solutions and  $\text{NaSO}_4$  solutions**

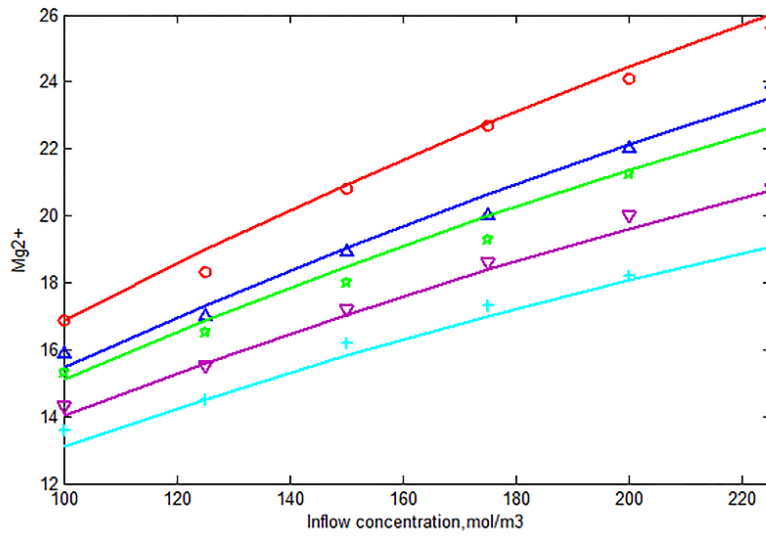


**Fig. 3. The experimental results and the prediction of  $Mg^{2+}$  concentration in steady-state solution as a function of inflow concentration at various energy inputs**

- and ○: The modelling curve and the experimental data with 0W, respectively
- and △: The modelling curve and the experimental data with 1.95W, respectively
- and ☆: The modelling curve and the experimental data with 3.88W, respectively
- and ▽: The modelling curve and the experimental data with 5.83W, respectively
- and +: The modelling curve and the experimental data with 7.78W, respectively

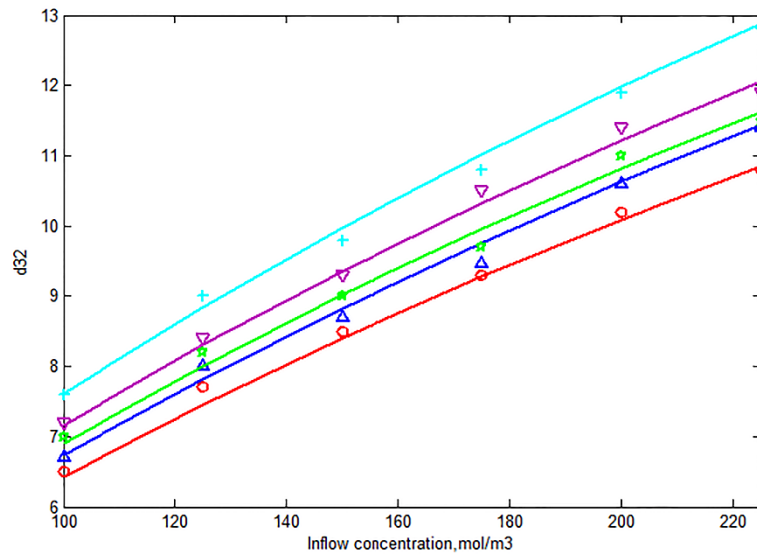


**Fig. 4. The experimental results and the prediction of  $d_{32}$  as a function of inflow concentration at various energy inputs**

- and  $\circ$ : The modelling curve and the experimental data with 0W, respectively
- and  $\triangle$ : The modelling curve and the experimental data with 1.95W, respectively
- and  $\star$ : The modelling curve and the experimental data with 3.88W, respectively
- and  $\nabla$ : The modelling curve and the experimental data with 5.83W, respectively
- and  $+$ : The modelling curve and the experimental data with 7.78W, respectively

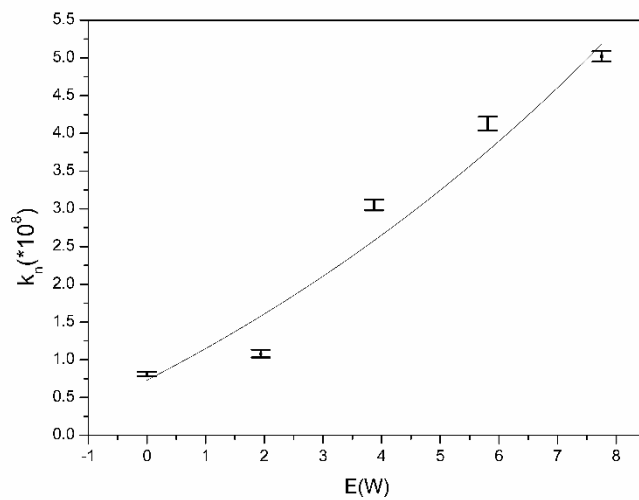


**Fig. 5.** The nucleation rate constant ( $k_n$ ) as a function of microwave energy inputs ( $E$ )

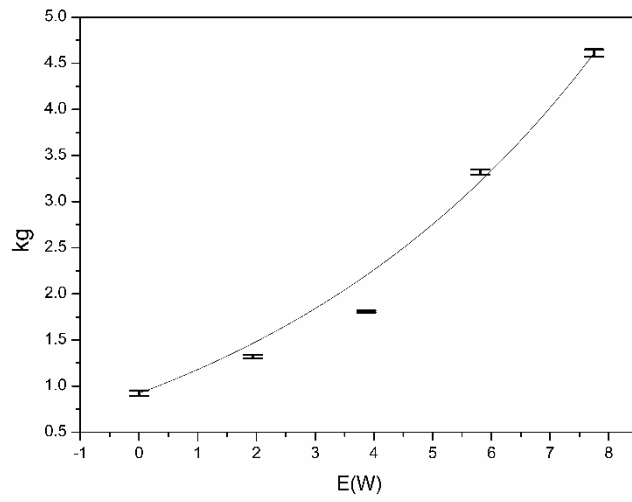


**Fig. 6.** The growth rate constant ( $k_g$ ) as a function of microwave energy inputs( $E$ )

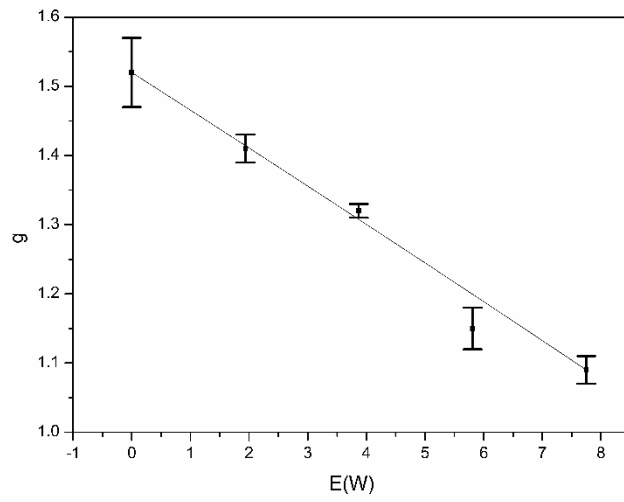


**Fig. 7. The exponent of growth rate ( $g$ ) as a function of the microwave energy input ( $E$ )**

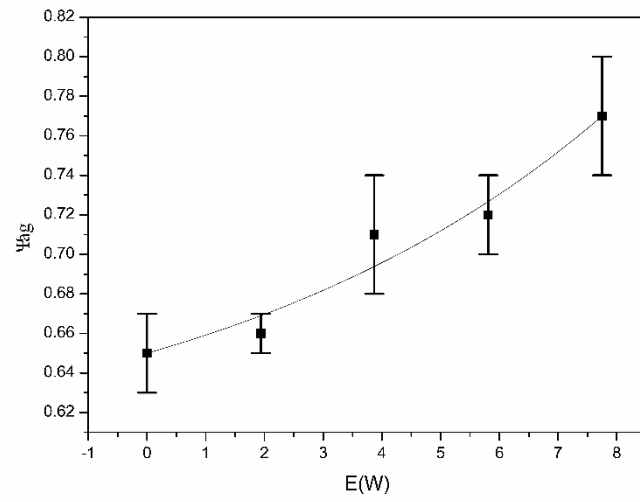


**Fig. 8.** The collision efficiency ( $\Psi_{ag}$ ) as a function of microwave energy inputs ( $E$ )

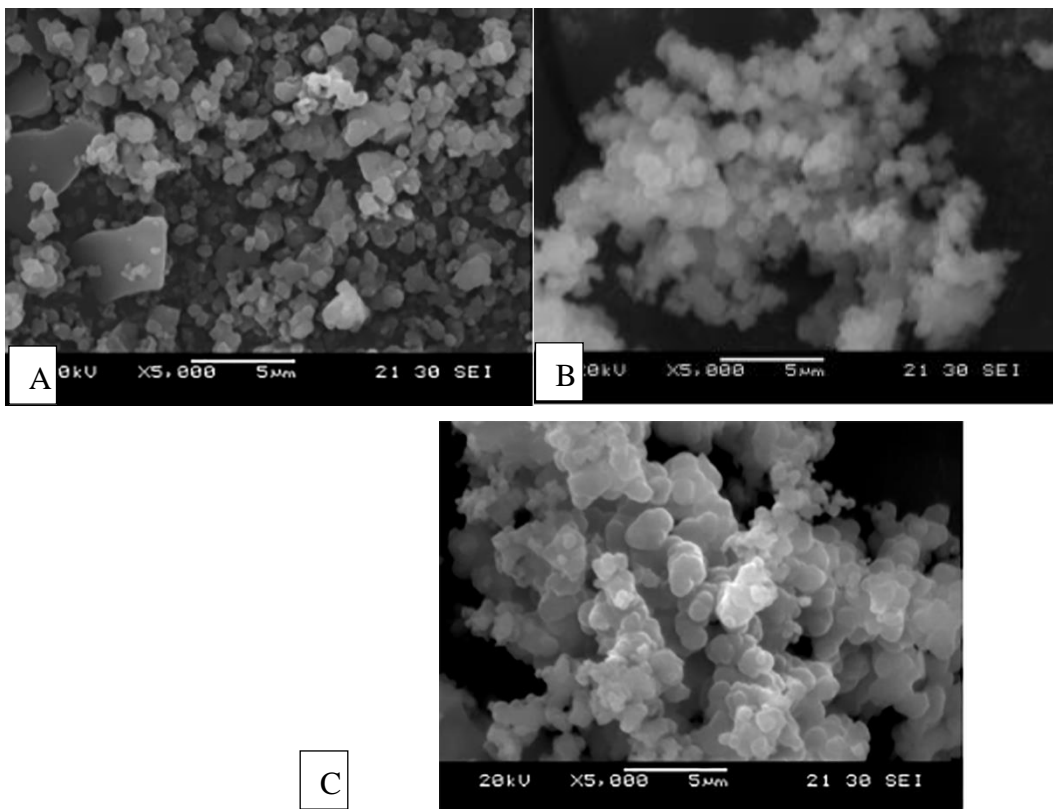


**Fig. 9. The SEM images of MgCO<sub>3</sub> crystals with various microwave energy inputs and inflow concentrations**

A: with the energy input of 0W and the inflow concentration of 0.1 mol/L

C: with the energy input of 7.78W and the inflow concentration of 0.1 mol/L

E: with the energy input of 7.78W and the inflow concentration of 0.225 mol/L

**Tables:****Table 1 Initial process parameters and physical properties of system**

Initial parameters	Values	Units
$\varepsilon$	$4.61 \times 10^{-2}$	J/kg/s
$\rho_L$	998.2	kg/m <sup>3</sup>
$\rho_{MgCO_3}$	$2.96 \times 10^3$	kg/m <sup>3</sup>
$k_{br}$	$6.0 \times 10^{-5}$	-
$T$	298	K
$\gamma$	0.74	-
$\Gamma_{50}$	0.63	-
$\alpha$	$1.50 \times 10^{11}$	Pa
$f_v$	$\pi/6$	-
$f_s$	$\pi$	-
$K_{sp}$	6.82	mol <sup>2</sup> ·m <sup>-6</sup>
$Q_{in}$	$3.25 \times 10^{-7}$	m <sup>3</sup> /s
$Q_{out}$	$6.50 \times 10^{-7}$	m <sup>3</sup> /s

**Table 2 Different microwave energy input vs the crystallization kinetic parameters obtained from simulation**

Energy input(E)	0W	1.94W	3.87W	5.81W	7.78W
$g$	1.52±0.05	1.41±0.02	1.32±0.01	1.15±0.03	1.09±0.02
$n$	6.01±0.04	6.09±0.07	6.03±0.02	6.04±0.06	6.05±0.03
$k_n$	(0.81±0.03)× 10 <sup>8</sup>	(1.08±0.05) × 10 <sup>8</sup>	(3.05±0.07) × 10 <sup>8</sup>	(4.13±0.09) × 10 <sup>8</sup>	(5.02±0.07) × 10 <sup>8</sup>
$k_g$	(0.92±0.03) × 10 <sup>-10</sup>	(1.32±0.02)× 10 <sup>-10</sup>	(1.81±0.01)× 10 <sup>-10</sup>	(3.32±0.03)× 10 <sup>-10</sup>	(4.61±0.04)× 10 <sup>-10</sup>
$\Psi_{ag}$	0.65±0.02	0.66±0.01	0.71±0.03	0.72±0.02	0.77±0.03
$k_{br}$	0.51±0.02	0.53±0.01	0.52±0.02	0.51±0.01	0.51±0.02